Dalton Transactions

Accepted Manuscript

ROYAL SOCIETY OF CHEMISTRY

www.rsc.org/dalton

Synthesis and transition metal coordination chemistry of a novel hexadentate bispidine ligand

Peter Comba, Henning Rudolf and Hubert Wadepohl*

Universität Heidelberg, Anorganisch-Chemisches Institut, INF 270, D-69120 Heidelberg, Germany

Correspondence:

e-mail: peter.comba@aci.uni-heidelberg.de

Fax: +49-6221-546617

Abstract.

Reported is the new bispidine-derived hexadentate ligand L (L = 3-(2-methylpyridyl)-7-(bis-2-methylpyridyl)-3,7-diazabicyclo[3.3.1]nonane) with two tertiary amine and four pyridine donor groups. This ligand can form heterodinuclear and mononuclear complexes and, in the mononuclear compounds discussed here, the ligand may coordinate as a pentadentate ligand, with one of the bispyridinemethane-based pyridine groups un- or semi-coordinated, or as a hexadentate ligand, leading to a pentagonal pyramidal coordination geometry or, with an additional monodentate ligand, to a heptacoordinate pentagonal bipyramidal structure. The solution and solid state data presented here indicate that, with the relatively small Cu^{II} and *high-spin* Fe^{II} ions the fourth pyridine group is only semi-coordinated for steric reasons and, with the larger *high-spin* Mn^{II} ion genuine heptacoordination is observed but with a relatively large distortion in the pentagonal equatorial plane.

Introduction.

The 3,7-diaza-bicyclo[3.3.1]nonane (bispidine) motif offers a rigid ligand backbone, resulting in a high degree of preorganization and rigidity, combined with a wide synthetic variability for tailor-made ligand systems. The bispidine itself was first discovered by Mannich and Mohs[1] and appears as a substructure of the natural product sparteine. The general synthesis of bispidines involves two consecutive double Mannich reactions via the piperidone intermediate.[1] Based on the possibility to enforce specific coordination geometries and therefore stabilize complexes with specific properties,[2, 3] the bispidine transition metal coordination chemistry has developed into a particularly broad field, with applications in catalytic aziridination,[4-6] sulfoxidation[7-9] and C-H-activation processes,[10-12] molecular magnetism,[13-16] the development of new ionophores,[17] radiotracers for positron emission tomography (PET),[18-20] and copper sensors.[21, 22] Typical bispidine ligands and the main structural features of their transition metal complexes are shown in Chart 1.

<Chart 1: Ligands discussed in this publication, and the two isomeric hexacoordinate structures with L^2 and L (if X = void), as well as the two coordination modes (mono- and dinucleating) of the hexadentate bispidine L.>

Here, we present the new bispine ligand L with a bis(2-pyridyl)methyl substituent, leading to a hexadentate ligand, an isomer of the known hexadentate bispidine L^2, with strikingly different complexing properties: this ligand can either coordinate to a single metal ion, leading to a pentagonal pyramidal structure and possibly to heptacoordination, when a monodentate ligand completes the distorted pentagonal bipyramidal coordination sphere, or behave as a dinucleating ligand (see Chart 1). We discuss two different synthesis strategies for the ligand - the classical double Mannich reaction sequence and the alkylation of the secondary amine at N7 of the tetradentate bispidone precursor. Also, in order to suppress retro Mannich ligand decay and hence enhance the stability of the formed complexes, ligand L was reduced at C9 to produce the corresponding alcohol derivative L^{OH}. Here, we report the first row transition metal coordination chemistry of the new bispidines as mononucleating ligands, and in particular we discuss the solid state and solution structures based on X-ray crystallography, electrochemistry and EPR as well as ligand field spectroscopy.

Results and Discussion.

Ligand synthesis.

The typical procedure to build up a bispidone is by two consecutive double Mannich reactions. The precursor for the synthesis of the desired ligand L, the known di(2-pyridyl)amine (2), obtained in a

two-step procedure from the commercially available di(2-pyridyl)ketone.[23] This was reacted with the common Npy_2 piperidone (pL) to obtain the L in up to 16% yield (Scheme 1). Due to the modest yield, L was alternatively obtained by alkylation of the secondary amine N7 of the bispidine precursor with the halogenated dipyridyl building block (Scheme 1). For this convergent synthesis, we decided to insert a latent benzyl protecting group at N7 by choosing benzyl amine as the amine component in the second Mannich reaction.[17] The resulting benzylated bispidine (5) was hydrogenated with palladium on activated charcoal, to remove the benzyl group and yield the secondary amine precursor (6). The di(2-pyridyl)methyl chloride (4) was obtained by a slightly modified published procedure,[24] where the di(2-pyridyl)ketone was reduced to the corresponding alcohol (3) with sodium boron hydride and subjected to an Apple reaction, to obtain the di(2-pyridyl)methyl chloride (4). After refluxing the bispidine precursor (6) with the chloride (4) in acetonitrile with sodium carbonate as base and a catalytic amount of sodium iodide, the desired ligand L was obtained in yields up to 53%, i.e. this procedure is clearly more efficient than the double Mannich reaction. Reduction of the ketone L at C9 to the corresponding alcohol L^{OH} with sodium borohydride, to prevent the retro Mannich reaction, resulting in ligand decomposition under acidic (pH < 3) or alkaline conditions (pH > 10), produced (L^{OH}) in 93% yield.

<Scheme 1: Two different synthetic routes to Ligand L.>

<Scheme 2: Reduction of L to L^{OH}>

Transition Metal Coordination Chemistry.

All synthesis were carried out under ambient conditions in methanol, if not mentioned otherwise. Equimolar solutions of the ligand and the metal salt were combined and stirred at room temperature overnight. Suitable crystals for X-ray crystal structure determination were obtained by diffusion of diethylether into the methanolic complex solutions.

Copper Complexes.

In the structures of the Cu^{II} complexes $[Cu^{II}(L)]^{2+}$ and $[Cu^{II}(L^{OH})]^{2+}$, shown in Figure 1 (selected structural data presented in Table 1), only five donors of the hexadentate ligands are coordinated (in both cases, a fluorine atom of the tetrafluoroborate counteion is interacting with Cu^{II} at the open position *trans* to N7 with a Cu-F distance of approx. 2.6 Å, see Table 1). One of the two pyridine groups attached to N7 (py4) is dangling, similar to the phenyl group in the analogous pentadentate

ligand L^3 (see Chart 1), from which structures of hexacoordinate Fe^{II} complexes similar to those in Figure 1 – with one monodentate ligand trans to N7 – are known.[25] That is, the coordination geometry around Cu^{II} is comparable to that observed with L^1 (see Table 1).[4, 26, 27] However, the dangling pyridine donor py4 of L and L^{OH} clearly points in the direction of the Cu^{II} center with a Cu···N distance of 3.89 Å and 3.85 Å (L and L^{OH}, respectively), which is an important difference to the structure of the Fe^{II} complex with L^3.[25] The third pyridine donor py3 is coordinated *trans* to N3, and this defines the pseudo-Jahn-Teller axis along Cu-N7. Since the second apical position is unoccupied in contrast to the structures with L^1, the Cu-N7 distances are as expected comparably short (see Table 1) – the pseudo-Jahn-Teller axis of the complex with the hexadentate isomer of L, L^2 (also presented in Table 1), is oriented along the py1-Cu-py2 axis. Interestingly, the position of the py3 donor in $[Cu^{II}(L)]^{2+}$ and $[Cu^{II}(L^{OH})]^{2+}$ is significantly different to that in $[Cu^{II}(L^1)Cl]^+$, with a shorter Cu-N distance (1.98 Å, 1.98 Å vs. 2.03 Å) and a compressed py1-Cu-py3 angle (96.2°, 96.0°, vs. 110.0°). Together with the significant tilt of the Cu-N7 axis with respect to the CuN_4 plane (increase of the py1-Cu-N7 angle of approx. 15°), this indicates that the particular distortion may be due to the Cu···py4 interaction and that the pentagonal-pyramidal coordination geometry (hexacoordination of L and L^{OH}) is prevented by ligand-induced strain (crowding in the basal plane due to relatively short metal-donor diatances), i.e., a larger metal ion could lead to the desired coordination geometry.

<Table 1: Selected distances and angles of the Cu^{II} complexes of L and L^{OH} in comparison with those of L^1 and L^2.[4, 28]>

<Figure 1: ORTEP plots of $[Cu^{II}(L)]^{2+}$ (left) and $[Cu^{II}(L^{OH})]^{2+}$ (right), hydrogen atoms are omitted for clarity, ellipsoids are shown with 50% probability.>

The redox potentials and electronic properties of the new complexes and of selected reference compounds are listed in Table 2. It appears that as a whole, the solution properties are very similar to those of the L^1-based Cu^{II} complex and therefore, we conclude that the solution structure is similar to that in the solid (see Figure 1), i.e. square pyramidal (or pseudo-octahedral) with a dangling but weakly interacting py4. This is supported by the axial EPR spectrum (see Figure 2) and the spin Hamiltonian parameters. As expected, the ligand field of the Cu^{II} complex is slightly reduced by reduction of the ligand from L to L^{OH}, and the redox potentials are consequently more positive (destabilization of the Cu^{II} state).[29] More importantly, the ligand field excerted by L is significantly smaller than that of L^1, and the corresponding redox potentials therefore are less negative, i.e. Cu^{II} is less stabilized by L than by L^1. This is in agreement with the structural properties enforced by L, i.e. the weak interaction of py4 leads to a distortion of the pseudo-square pyramidal coordination geometry.

<Table 2: Redox potentials (MeCN vs. Fc/Fc+, vs. Ag/$AgNO_3$; H_2O vs. $K_3[Fe(CN)_6]$ [a] or vs. Ag/AgCl[b]) and spectroscopic data of the Cu^{II} complexes of L and L^{OH}, in comparison with other Cu^{II} bispidine complexes.[4, 28-30] >

<Figure 2: X-band EPR spectrum of $[Cu^{II}(L)]^{2+}$ in MeOH/EtOH (9:1) at 5 K and 9.423336 GHz, black line (bottom): experimental spectrum, red line (top) simulated spectrum.>

Due to the fact that the stability constants of Cu^{II} complexes vary over a wide range and those of Cu^{I} are much less variable, there is an approximate in linear correlation between $Cu^{II/I}$ redox potentials and the corresponding Cu^{II} stability constants.[31] For ligands with a similar organic backbone and a constant donor set, this type of correlation offers an ideal possibility for an accurate prediction of stability constants and, for the very rigid bispidine scaffold it has been demonstrated that this is the case.[30, 32] Based on these established correlations and the redox potentials reported in Table 2, the expected stability constants for the two complexes are log*K*{$[Cu^{II}(L)]^{2+}$} = 16.0 and log*K* {$[Cu^{II}(L^{OH})]^{2+}$} = 16.3 (see Supporting Information). As discussed above, these values are comparable but slightly smaller than the experimentally determined value for $[Cu^{II}(L^1)]^{2+}$, and we believe that this is due to the distortion induced by semi-coordination of py4.

Iron Complexes.

Most of the reported Fe^{II} bispidine complexes exist in an S=2 spin state (*high spin*), most are close to the spin crossover limit, and only one genuine *low spin* (S=0) complex has been reported so far;[29, 33, 34] *intermediate spin* (S=1) electronic configuration is extremely rare for Fe^{II} and may be imposed by a pentagonal bipyramidal coordination geometry. The generally larger metal donor distances with *high spin* Fe^{II} compared to Cu^{II} (approx. 2.2 vs. 2.0 Å for amine donors) leads to the expectation that L might enforce seven-coordination and a distorted pentagonal bipyramidal geometry with Fe^{II}. From the two crystal structures of $[Fe^{II}(L)X]^{n+}$ complexes (X=Cl, OHMe, see Figure 3 and Table 3) obtained, it emerges, however, that the fourth in-plane pyridine donor (py4), similar to the Cu^{II} structures discussed above, is dangling but with an even shorter distance to the metal center (3.03 Å vs. 3.85 Å) and therefore may be considered semi-coordinated. Also presented in Figure 3 and Table 3 is an Fe^{III} complex of L, obtained by reaction of the ligand with an Fe^{II} salt under ambient conditions – all other complexation reactions were performed under inert atmosphere. For comparison, selected structural data of other iron-amine / pyridine complexes are listed in Table 3.

<Figure 3: ORTEP plots of the complex cations (a) $[Fe^{II}(L)OHMe]^{2+}$, (b) $[Fe^{II}(L^{OH})Cl]^{+}$, and (c) $[Fe^{III}(L)OMe]^{2+}$; hydrogen atoms are omitted for clarity, ellipsoids are shown with 50% probability level. >

< Table 3: Selected bond distances and angles of the Fe^{II} and Fe^{III} complexes of L, L^{OH} and other bispidine complexes.>

In the structures of the Fe^{II} complexes of L and L^{OH}, an octahedral coordination geometry is completed by a monodentate Cl^- or methanol solvent molecule, respectively, coordinated *trans* to N7, completing the coordination sphere. Semi-coordination of py4 again leads to a distortion of the remaining Fe^{II}-N_2py_3X chromophore, similar to but more pronounced as that discussed above for the Cu^{II} complexes, in particular for the unreduced L-based system (reduction of the ketone leads to a slight increase of the donor strength; the discussion refers to the ketone-based ligand L):[27-29] (i) the data in Table 3 suggest that the Fe···py4 interaction tends to reduce the Fe-N7 distance (and concomitantly increases the Fe-N3 distance);[28, 30] (ii) the Fe···py4 interactions leads to an asymmetry with respect to the coordination of two pyridine donors py1 and py2, i.e., the two angles py1,2-Fe-py3 are strikingly different (85° vs. 137° and 87° vs. 130°, respectively).

Due to problems with the solubility of the various complexes, the redox potentials (see Table 4) could not all be determined in the same solvent, and the electronic spectra in solution (also given in Table 4) are, as expected for *high spin* Fe^{II} systems, relatively feature-less and therefore not fully assigned. Qualitatively, it appears however, that there is a significant difference between the solution properties of the complexes with L and L^{OH} in comparison to the complexes of the analogues L^1, L^2 and L^3, suggesting also a semi-coordination of the additional pyridine group py4. Specifically, there is the expected reduction of the ligand field and a concomitant destabilization of the reduced Fe^{II} form.

< Table 4: Redox potentials (MeCN vs. Fc/Fc+ [a)]; vs. $Ag/AgNO_3$ [b)]; H_2O vs. $K_3[Fe(CN)_6]$ [c)]; vs. Ag/AgCl [b)]) and spectroscopic data of the Fe^{II} complexes of L and L^{OH}, in comparison with other Fe^{II} bispidine complexes.[33, 35, 36]

Interestingly, when the complex synthesis is performed under ambient atmosphere, spontaneous oxidation of the Fe^{II} complex to Fe^{III} takes place,[37] and the corresponding complex could be isolated and crystallized; the structures of the molecular cations are also shown in Figure 3 and selected structural parameters are given in Table 3 together with those of a similar published structure with another pentadentate bispidine ligand $L^{1'}$ ($L^{1'}$ is an isomer to L^1 with the pyridine group attached to N3 instead of N7). The complex has the expected distorted octahedral geometry with L coordinated as a tetradentate ligand to a *high spin* Fe^{III} center with a semi-coordinated py4 donor. The metal donor distances are very similar to those of the corresponding *high spin* Fe^{II} complex (see Table 3) but, as in the similar $L^{1'}$ based system, the OMe^- donor, coordinated as an anionic coligand has, as expected, a relatively short metal-ligand bond (Fe^{III}-O = 1.79 Å). Other Fe^{III} methoxy complexes with similar amine / pyridine ligands (e.g. N4py = *N,N*-bis(2-pyridyl)methyl)-*N*-(bis-2-pyridylmethyl)amine[39] and bztpen = *N*-benzyl-*N,N',N'*-tris(2-methylpyridyl)ethylendiamine)[40] have similar structural features, especially also with respect to the Fe-O-CH_3 angle of 149°, which is

typical for a *high spin* Fe^{III} electronic configuration:[33, 34, 39, 40] typical Fe-O-CH_3 angles for *low spin* Fe^{III} are around 130°, those for *high spin* Fe^{III} are around 150-170°.[38, 39]

Confirmation of the electronic ground state in solution arises from magnetic moment determinations (Evans-NMR, CD_3CN). For the two *high spin* Fe^{II} complexes, the effective magnetic moments are: μ_{eff} = 4.9612 B.M. for $[Fe^{II}(L)OHMe]^{2+}$ and μ_{eff} = 4.8734 B.M. for $[Fe^{II}(L^{OH})Cl]^{+}$, and this is typical for *high spin* d^6 configuration, with S = 2 and a spin only moment of μ_{eff} = 4.899 B.M.. The magnetic moment of $[Fe^{III}(L)OMe]^{2+}$ in solution is μ_{eff} = 5.1882 B.M., typical for a *high spin* d^5 (S = 5/2) electronic ground state with a spin only moment of μ_{eff} = 5.916 B.M..

Manganese Complexes.

There are a number of Mn^{II} bispidine complexes known, especially with tetradentate bispidine ligands and, as expected for *high spin* d^5 systems, their geometries are generally octahedral with Mn-N distances significantly larger than those of the Fe^{II} complexes.[27, 29, 41] Therefore and since heptacoordinate Mn^{II} complexes (pentagonal bipyramidal and monocapped trigonal prismatic) are not uncommon,[42-44] the hexacoordinating bispidine L was coordinated to Mn^{II}. Diffusion of diethylether into the methanolic solution of $[Mn^{II}(L)Cl]^{+}$, obtained by the combination of a methanolic solution of $MnCl_2$ with an equimolar amount of ligand, produced practically colorless needles, suitable for X-ray diffraction. A plot of the molecular cation of $[Mn^{II}(L)Cl]^{+}$, obtained by X-ray crystal structure analysis, is shown in Figure 4; selected structural parameters are presented in Table 5, which also lists relevant data for comparison (there are two independent complex cations, in the unit cell, and the parameters of both are tabulated).

< Figure 4: (a) ORTEP plot of the complex cation $[Mn^{II}(L)(Cl)]^{+}$ (hydrogen atoms are omitted for clarity, ellipsoids are shown with 50% probability level); (b) overlay plot of $[Mn^{II}(L)(Cl)]^{+}$ (red, M=Mn^{II}) and $[Fe^{II}(L)(HOMe)]^{2+}$ (green, M=Fe^{II}).>

< Table 5: Selected structural parameters of $[Mn^{II}(L)Cl]^{+}$ and relevant data for comparison.>

As hoped for, the structure of $[Mn^{II}(L)(Cl)]^{+}$ is heptacoordinated with the hexacoordinating bispidine and a Cl^{-} completing the distorted pentagonal bipyramidal coordination sphere. In terms of the coordination of the two dipyridinamine-based pyridine donors py3 and py4, the structure is, due to ligand-enforced strain, still significantly distorted but the longer Mn-py3,4 distances of 2.34, 2.4, 2.53 and 2.65 Å all can be considered as genuine bonds. The *trans* angle N7-Mn-Cl 165° (167°) is in agreement with a (distorted) bipyramidal structure. The intra-donor angles in the pentagonal plane indicate a relatively symmetrical distribution with an ideal value of 72° and an observed distribution between 67° and 82°, and the average deviation of 0.38 Å from a mean plane is significant but not very large. The most extensive distortion is related to the position of N3 (rigid N3-Mn-N7 angle) and

the two pyridine groups py3 and py4 (tight and rigid chelate rings involving N7 and py3, py4), and this results in N3, py3, py4 all being above the mean equatorial plane (0.57 Å, 0.06 Å, 0.19 Å, respectively, all for molecule 1; Mn is by 0.38 Å above the plane; py1 and py2 are by 0.49Å and 0.35Å below the plane; the corresponding values for molecule 2 are similar, see ESI). As a result, the repulsion between the pyridyl groups py3 (and py4) and the α hydrogen atoms of py1 (and py2) is reduced. In order to visualize the similarity between the 7-coordinated Mn^{II} and the 6-coordinated Fe^{II} structures and to justify the "semi-coordination" of py4 in the Fe^{II} and Cu^{II} structures, an overlay plot of $[Mn^{II}(L)(Cl)]^{+}$ and $[Fe^{II}(L)(HOMe)]^{2+}$ is also shown in Figure 4.

The redox potential ($Mn^{II/III}$ couple vs. SCE) of $[Mn^{II}(L)(Cl)]^{+}$ is significantly more positive than that of the hexacoordinate $[Mn(tpen)Cl]^{+}$ with a similar donor set, indicating that the extra pyridine donor prevents oxidation and concomitant compression of the coordination sphere. For the 7-coordinated EDTA and NOTA complexes with H_2O as an extra ligand, steric effects are of lesser importance (possible dissociation of the 7^{th} ligand and reduction of the coordination number) and the carboxylates obviously stabilize the oxidized form.

< Table 6: Redox potentials of $[Mn(L)Cl]^{+}$ relevant data for comparison in MeCN, vs. SCE.>

Squid magnetometry was used to analyze the electronic ground state of $[Mn^{II}(L)(Cl)]_2[MnCl_4]$ (Figure 5). It follows that the zero field splitting is neglectable and the magnetic suszeptibility at room temperature per $[Mn^{II}(L)(Cl)]^{+}$ cation (S = 5/2 for the $[MnCl_4]^{2-}$ complex ion)[45] is 4.168 cm^3 K mol^{-1}, typical for a *high spin* d^5 center (S=5/2, 4.337 cm^3 K mol^{-1} for g=2). It appears that spin pairing to result in possible S = 3/2 (*intermediate spin*) and S = ½ (*low spin*) states, due to (distorted) pentagonal bipyramidal coordination geometry, is prevented by the long metal-donor distances and the resulting relatively weak ligand field.

<Figure 5: (a) Temperature depencent suszeptibility and (b) reduced magnetization of $[Mn^{II}(L)(Cl)]_2[MnCl_4]$.>

Conclusion.

The hexadenate bispidine ligands L and L^{OH} have been shown to be able to form heptacoordinated pentagonal bipyramidal structures. For the relatively small Cu^{II} and *high spin* Fe^{II} ions the fourth pyridine group is only semi-coordinated for steric reasons and, with the larger *high spin* Mn^{II} ion genuine heptacoordination is observed but with a relatively large distortion in the pentagonal equatorial plane. It appears that an elongation of chelate rings involving the dipyridylamine group

might lead to the desired enforcement of pentagonal (bi)pyramidal structures, even for smaller metal ions, and this also emerges from similar effects observed with 6- vs. 5-membered chelate rings involving the N7-appended pyridine donor in L^1-based pentadentate bispidine ligands.[46, 47] Moreover, an expansion of the linker between N7 and the pyridine donors py3 and py4 would also lead to less distortion in the equatorial plane, even with relatively large metal-donor distances.

Experimental Section.

All chemicals were purchased from Sigma Aldrich and Acros. Analytical grade solvents were used without further purification and all reactions were carried out under air if not mentioned otherwise. The piperidone precursor pL was synthesized according to a published procedure.[29]

Caution! Metal perchlorates in presence of organic ligands are potentially explosive and sensitive to heat and impact. No problem occurred for the work described here but these compounds need in general to be handled with extreme care.

Electrochemistry was performed on a CH Instruments CHI660D electrochemical workstation, equipped with a CH Instruments Picoamp Booster. All electrochemical measurements were performed in a glass cell, covered with a teflon cap, situated in a Faraday cage. All complex solutions were prepared in degassed and with Argon saturated solvents. The supporting electrolyte for non-aqueous solutions were: for methanol (MeOH): 0.1M tera-*n*-butylammonium tetrafluoroborate; for acetonitrile (MeCN): 0.1M tera-*n*-butylammonium hexafluorophosphate. Cyclovoltammograms (CVs) in non-aqueous media were recorded with an $Ag/AgNO_3$ reference electrode, a glassy carbon working electrode and a platinum wire as counter electrode. Aqueous solutions contained 3M sodium chloride (NaCl) as supporting electrolyte and were measured with an Ag/AgCl reference electrode, a glassy carbon working electrode and a platinum wire as counter electrode. Electrochemical measurements in non-aqueous media were normalized vs. ferrocene, where ferrocene had the following potential: MeCN (50mV); in H_2O, potentials were normalized against potassium hexacyano ferrate ($K_3[Fe(CN)_6]$) with 270mV.

UV/vis spectra were recorded with a Jasco V-570 UV-vis-NIR spectrometer as methanolic solutions.

NMR spectra were recorded with a Bruker Avance I (200MHz) instrument; chemical shifts of ^1H and ^{13}C were referenced to solvent resonances ($CDCl_3$).

ESI-MS spectra were recorded on a Bruker ApexQe hybrid 9.4 T FT-ICR instrument.

Elemental analysis were obtained from a CHN-O-vario EL instrument by the "Mikroanalytisches Labor" of the chemical institutes, University of Heidelberg.

EPR measurements were performed on a Bruker ELEXSYS-E-500 instrument and collected at liquid helium temperature in frozen methanol/ethanol (9:1) solution. The spin Hamiltonian parameters were obtained by simulation of the experimental data with the XSophe software package.[48, 49]

X-ray Crystal Structure Determinations. Crystal data and details of the structure determinations are listed in the ESI (Table S3). Full shells of intensity data were collected at low temperature with a Bruker AXS Smart 1000 CCD diffractometer (Mo-*K*α radiation, sealed tube, graphite monochromator; compounds $[Fe^{II}(L)OHMe]^{2+}$ and $[Fe^{III}(L)OMe]^{2+}$) or a Agilent Technologies Supernova-E CCD diffractometer (Mo- or Cu-*K*α radiation, microfocus tube, multilayer mirror optics; compounds $[Cu^{II}(L)]^{2+}$, $[Cu^{II}(L^{OH})]^{2+}$ and $[Fe^{II}(L^{OH})Cl]^{+}$) or STOE IPDS I diffractometer (Mo-*K*α radiation, graphite monochromator; compound $[Mn^{II}(L)Cl]^{+}$). Data were corrected for air and detector absorption, Lorentz and polarization effects;[50, 51] absorption by the crystal was treated numerically (Gaussian grid)[51] (compounds $[Cu^{II}(L)]^{2+}$ and $[Cu^{II}(L^{OH})]^{2+}$) or with a semiempirical multiscan method[3, 52, 53] (all others).The structures were solved by conventional direct methods[54, 55] (compound $[Mn^{II}(L)Cl]^{+}$) or by the charge flip procedure[56, 57] (all others) and refined by full-matrix least squares methods based on F^2 against all unique reflections.[55, 58] All non-hydrogen atoms were given anisotropic displacement parameters. Hydrogen atoms were generally input at calculated positions and refined with a riding model. Where possible, hydrogen atoms of solvent water were taken from difference Fourier syntheses or else placed to maximize hydrogen bonding[59, 60] with atomic charges calculated from partial equalization of orbital electronegativity.[61] Water molecules were then refined as rigid groups. When found necessary, disordered groups and/or solvent molecules where subjected to suitable geometry and adp restraints.

In the structure of $[Fe^{II}(L^{OH})Cl]^{+}$ a cluster of 3 strong difference Fourier peaks was assigned to partially occupied sites of the chloride ion. Their total population refined to close to 1.0. The smtbx solvent masking procedure was then used to remove the electronic contribution of residual solvent molecules (water and/or methanol) from the F_{obs}.[62, 63] During refinement against the solvent-corrected data the sum of populations for the chlorides was restrained to 1.00(1). Due to severe disorder and fractional occupancy, electron density attributed to solvent of crystallization (methanol and/or water) was removed from the structure of $[Mn^{II}(L)Cl]^{+}$ with the BYPASS procedure,[62] as implemented in PLATON (SQUEEZE).[64, 65] Partial structure factors from the solvent masks were included in the refinement as separate contributions to F_{obs}.

Syntheses.

Di(2-pyridyl)oxime.[66, 67] ($C_{11}H_9N_3O$, MW: 199.21 g/mol): To sodium acetate (2.96 g, 21.71 mmol, 2 eq) in water (20.00 ml) was added hydroxylamine hydrochloride (1.51 g, 21.71 mmol, 2 eq) and heated to 60 °C for one hour. Di(2-pyridyl)ketone (2.0 g, 10.86 mmol, 1 eq) was added in methanol (4.0 ml) and the brown solution was stirred at 60 °C overnight. The light red reaction mixture was cooled at 0 °C and the product precipitated in light-rose crystals. The product (2.10 g, 97 % yield) was filtered, washed with a little cold water and dried in vacuo. FAB-MS: m/z = 200.10 (calc: 200.08) $[M+H]^+$; elemental analysis (report no. : 28891, $C_{11}H_{11}N_3O_2$) calc: C(60.82), H(5.10), N(19.34), obs: C(61.10), H(5.04), N(19.28).

Di(2-pyridyl)methylamine. ($C_{11}H_{11}N_3$, MW: 185.23 g/mol) The di(2-pyridyl)oxime (2.08 g, 10.44 mmol, 1 eq), ammonium acetate (1.37 g, 17.75 mmol, 1.7 eq) and concentrated ammonia (3.3 ml) were dissolved in ethanol/water (2:1, 63.0 ml) and heated to 80 °C. Zinc dust (3.07 g, 47.0 mmol, 4.5 eq) was added in small portions during 30 minutes and the mixture was refluxed for additional 3 hours. After stirring at room temperature overnight, solids were removed by filtration, washed with a little water, and ethanol was removed at the rotary evaporator. The remaining solution was alkalized with 10 M sodium hydroxide solution and the amine was extracted with methylene chloride. The combined extracts were washed with brine, dried over sodium sulfate and evaporated. The crude product (1.37 g, 71 % yield), a yellow-brown oil was used without further purification. ^{1}H-NMR (400MHz, $CDCl_3$) δ[ppm]= 2.50 (br s, N**H**$_2$, 2H), 5.34 (m, C**H**, 1H), 7.14-7.17 (m, **H**$_{arom.}$, 2H), 7.39-7.41 (m, **H**$_{arom.}$, 2H), 7.62-7.66 (m, **H**$_{arom.}$, 2H), 8.57-8.58 (m, **H**$_{arom.}$, 2H), ^{13}C-NMR (100 MHz, $CDCl_3$): δ[ppm]= 62.29, 121.73, 122.05, 136.66, 149.14, 162.69.

Di(2-pyridyl)methanol.[66, 67] ($C_{11}H_{10}N_2O$, MW: 186.21 g/mol): Sodium borohydride (1.03 g, 27.10 mmol, 1 eq) was added in small portions to a solution of di(2-pyridyl)ketone (5.00 g, 27.10 mmol, 1 eq) in methanol (50.0 ml) at 0 °C. The solution was warmed and stirred at room temperature overnight. The solvent was evaporated to dryness and the residue was taken up in water (20.0 ml) and acidified with 2 N hydrochloride acid. After stirring for 10 minutes, the solution was alkalized with concentrated ammonia and extracted with methylene chloride (3 x 50.0 ml). The combined organic extracts were dried with sodium sulfate and evaporated. The product (4.93 g, 98 % yield), a brown oil was dried in vacuuo and used without further purification. ^{1}H-NMR (200MHz, $CDCl_3$) δ[ppm]= 6.01 (s, C**H**, 1H),6.05 (s, O**H**, 1H), 7.22-7.30 (m, **H**$_{arom.}$, 2H), 7.60-7.64 (m, **H**$_{arom.}$, 2H), 7.70-7.77 (m, **H**$_{arom}$, 2H), 8.58-8.61 (m, **H**$_{arom.}$, 2H), ^{13}C-NMR (50 MHz, $CDCl_3$): δ[ppm]= 74.66, 121.65, 122.80, 125.10, 126.23, 136.62, 137.55, 147.56, 149.13, 154.53, 160.42.

Di(2-pyridyl)methyl chloride.[66, 67] ($C_{11}H_9ClN_2$, MW: 204.6 g/mol): To a solution of di(2-pyridyl)methanol (4.61 g, 24.76 mmol, 1 eq) in acetonitrile (52.0 ml) was added a solution of triphenylphosphine (7.79 g, 29.71 mmol, 1.2 eq) in carbon tetrachloride (42.0 ml) at 0 °C over a

period of 90 minutes drop wise. The solution was stored at +4°C overnight and quenched with methanol (6.0 ml) for 15 minutes at room temperature. The initial volume was concentrated to 25.0 ml, dissolved in water (52.0 ml) and washed with chloroform (2 x 52.0 ml). The aqueous phase was neutralized with potassium carbonate and extracted with diethyl ether (4 x 35.0 ml). The combined ether extracts were dried with sodium sulfate and evaporated. The crude product was obtained as a brown oil and purified by column chromatography (silica, 30 x 6 cm, methylene chloride/methanol 10:1, R_f 0.46). The analytically pure product was obtained as light-rose crystals (2.37 g, 47 % yield). ^{1}H-NMR (200MHz, $CDCl_3$) δ[ppm]= 6.24 (s, C**H**Cl, 1H); 7.14–7.21 (m, 2H); 7.61–7.74 (m, 4H); 8.48–8.51 (m, 2H); ^{13}C-NMR (50 MHz, $CDCl_3$): δ[ppm]= 63.76 (, 123.10, 137.36 , 148.79 , 158.29. , elemental analysis ($C_{11}H_9ClN_2$): calc: C(64.56), H(4.43), N(13.69), obs: C(64.48), H(4.56), N(13.54).

Dimethyl-(7-benzyl-3-methyl-9-oxo-2,4-bis(2-pyridyl)-3,7-diazabicyclo[3.3.1]nonane)-1,5-dicarboxylate. ($C_{29}H_{30}N_4O_5$, MW: 514.57 g/mol): Benzylamine (3.44 ml, 31.55 mmol, 1.2 eq) and formaldehyde (37 % wt in water, 4.7 ml, 63.09 mmol, 2.4 eq) were added to a suspension of the piperidone pL (10.0 g, 26.29 mmol, 1 eq) in ethanol (60.0 ml) and refluxed for 4 hours. The black solution was stirred overnight at room temperature and the precipitated product was filtered and washed with ethanol. After recrystallization from ethanol, the product was obtained as a white powder (6.69 g, 49 % yield). ^{1}H-NMR (200MHz, $CDCl_3$) δ[ppm]= 2.01 (s, C**H**$_3$, 3H), 2.56-2.62 (d, $^2J_{H\text{-}H}$ = 11.87 Hz, C**H$_{2,eq}$**, 2H), 3.06-3.13 (d, $^2J_{H\text{-}H}$ = 12.09 Hz, C**H$_{2,ax}$**, 2H), 3.40 (s, NC**H**$_2$Ph, 2H), 3.86 (s, OC**H**$_3$, 6H), 4.73 (s, C**H**, 2H), 7.13-7.20 (m, **H**$_{arom.}$, 2H), 7.43-7.55 (m, **H**$_{arom.}$, 7H), 7.90-7.94 (d, $^3J_{H\text{-}H}$ = 7.80 Hz, **H$_{arom.}$**, 2H), 8.46-8.49 (m, **H**$_{arom.}$, 2H), ^{13}C-NMR (50 MHz, $CDCl_3$): δ[ppm]= 43.26, 52.46, 59.01, 61.17, 62.47, 73.81, 122.87, 123.45, 127.65, 128.43, 130.42, 136.16, 136.94, 149.08, 158.47, 168.53, 203.65. ESI-MS:, elemental analysis ($C_{29}H_{30}N_4O_5$, report no.: 31987): calc. C(67.88), H(5.88), N(10.89), obs.: C(67.83), H(5.90), N(10.82).

Dimethyl-(3-methyl-9-oxo-2,4-bis(2-pyridyl)-3,7-diazabicyclo[3.3.1]nonane)-1,5-dicarboxylate.
($C_{22}H_{24}N_4O_5$, MW: 424.45 g/ mol) To a solution of Npy_2NBn (4.0 g, 7.77 mmol, 1 eq) in ethyl acetate (100.0 ml) was added palladium on activated charcoal (10%, 0.40 g) and the mixture was hydrated at 70 °C and 1 atm hydrogen overnight. The solvent was evaporated, the residue taken up in methylene chloride and the catalyst was removed by filtration over celite pad. After evaporation of the solvent, the crude product was recrystallized from ethanol as colorless needles (2.53 g, 77 % yield). ^{1}H-NMR (200 MHz, $CDCl_3$) δ[ppm]= 1.73 (s, NC**H**$_3$, 3H); 3.07-3.21 (m, C**H**$_{2\ ax/eq}$, 2H); 3.64 (s, OC**H**$_3$, 6H); 3.82-3.89 (m, C**H**$_{2\ ax/eq}$, 2H); 4.56 (s, C**H**, 2H); 7.18-7.20 (m, **H**$_{py}$, 2H); 7.33-7.37 (m, **H**$_{py}$, 2H); 7.59-7.67 (m, **H**$_{py}$, 2H); 8.60-8.62 (m, **H**$_{py}$, 2H) ppm. ^{13}C-NMR (50 MHz, $CDCl_3$) δ[ppm]= 41.61, 52.20, 55.06, 64.42, 73.73, 123.22, 124.39, 136.53, 150.05, 157.29, 168.70, 202.91. ESI-MS: m/z = 425.1 (100%), 426.1

(24%) $[M+H]^+$, elemental analysis ($C_{22}H_{24}N_4O_5$, report no.: 31986): calc.: C(62.25), H(5.70), N(13.20), obs.: C(62.39), H(5.75), N(13.20).

Dimethyl-(3-methyl-7-bis(2-pyridyl)methyl-9-oxo-2,4-bis(2-pyridyl)-3,7-diazabicyclo[3.3.1]nonane)-1,5-dicarboxylate (L) ($C_{33}H_{32}N_6O_5$, MW: 592.64 g/mol): *Method A:* To a suspension of the piperidone pL (2.74 g, 2.7 mmol, 1 eq) in methanol (15.0 ml) was added Di(2-pyridyl)methylamine (1.60 g, 8.64 mmol, 1.2 eq) and formaldehyde (37 % wt in water, 1.3 ml, 17.28 mmol, 2.4 eq) and was refluxed for 1 hour. After evaporation of the solvent, the residue was recrystallized from hot ethanol to obtain the product as a white powder (0.67 g, 16 % yield). *Method B:* Di(2-pyridyl)methyl chloride (0.50 g, 2.44 mmol, 1 eq) was refluxed for 24 hours with Npy_2NH (1.03 g, 2.44 mmol, 1 eq), sodium carbonate (0.52 g, 4.89 mmol, 2 eq) and a catalytic amount of sodium iodide in acetonitrile (10.0 ml). After complete evaporation of the solvent, the residue was partitioned between water and methylene chloride, the organic phase was separated, the aqueous phase was extracted with methylene chloride and the combined organic extracts were dried over sodium sulfate. After evaporation of the solvent the residue was recrystallized from ethanol to obtain the product as a white powder (0.76 g, 53 % yield). ^{1}H-NMR (200 MHz, $CDCl_3$) δ[ppm]= 1.89 (s, NC**H**$_3$, 3H), 3.03-3.09 (d, $^2J_{H\text{-}H}$ = 12.3 Hz, C**H$_{2,ax}$**, 2H), 3.46-3.52 (d, $^2J_{H\text{-}H}$ = 11.4 Hz, C**H$_{2,eq}$**, 2H), 3.67 (s, OC**H**$_3$, 6H), 4.47 (s, C**H**, 2H), 4.75 (s, NC**H**, 1H), 7.03-7.10 (m, **H**$_{py}$, 4H), 7.49-7.66 (m, **H**$_{py}$, 6H), 7.76-7.80 (d, $^3J_{H\text{-}H}$ = 7.8 Hz, **H**$_{py}$, 2H), 8.36-8.49 (m, **H**$_{py}$, 4H), ^{13}C-NMR (50 MHz, $CDCl_3$) δ[ppm]= 42.45, 52.36, 56.31, 63.08, 74.34, 77.95, 122.46, 122.84, 124.20, 124.48, 136.26, 149.08, 149,18, 157.90, 159.23, 168.82, 202.73., elemental analysis ($C_{33}H_{32}N_6O_5$, report no.: 32196): calc.: C(66.88), H(5.44), N(14.18), obs.: C(66.67), H(5.56), N(14.08).

Dimethyl-(3-methyl-7-bis(2-pyridyl)methyl-9-hydroxo-2,4-bis(2-pyridyl)-3,7-diazabicyclo[3.3.1]nonane)-1,5-dicarboxylate (L^{OH}). ($C_{33}H_{34}N_6O_5$, MW: 594.66 g/mol): The Ligand L (0.32 g, 0.54 mmol, 1 eq) was dissolved in 1,4-dioxane-water-mixture 3:1 (12.0 ml) an cooled to -5°C, sodium borohydride (0.01 g, 0.27 mmol, 0.5 eq) in 1,4-dioxane-water-mixture 2:1 (4.0 ml) was added drop wise. The solution was allowed to warm up to 0 °C and was stirred overnight. The solution was acidified with concentrated sulfuric acid until the solution remained clear. After stirring for 3 hours at 0 °C, the solution was alkalized with sodium hydroxide solution (20 % wt. in water) and L^{OH} was extracted with methylene chloride. After drying the organic extracts over sodium sulfate and evaporating the solvent, and recrystallizing from ethanol, the product was obtained as a white powder (0.30 g, 93 % yield). ESI-MS (pos): m/z = 595.2 $[L^{OH}+H]^+$, 617.3 $[L^{OH}+Na]^+$, elemental analysis ($C_{35}H_{40}N_6O_6$, report no.: 29984) calc. C(66.11), H(6.03), N(13.61), obs. C(66.01), H(5.77), N(13.83).

$[Cu^{II}(L)](BF_4)_2x3H_2O$. Solutions of L (100 mg, 168.73 µmol, 1 eq) in MeCN (4.0 ml) and dry $Cu(BF_4)_2$ (40 mg, 168.73 µmol, 1 eq) in MeCN (1.0 ml) were combined and the deep blue solution was refluxed

for 1 hour. The solvent was evaporated to dryness and the residue was taken up in MeOH and subjected to diethyl ether diffusion to obtain blue needles (104 mg, 74 % yield). UV/Vvis λ = 626 nm (15974 cm^{-1}), ε = 119 M^{-1} cm^{-1}; CV:-651 mV (MeCN vs. Fc/Fc^{+}), -786 mV (H_2O vs. $K_3[Fe(CN)_6]$), Elemental analysis (report no.: 32312): calc. (%): C(44.84), H(4.33), N(9.51); obs. (%):C(44.66), H(4.35), N(9.38).

$[Cu^{II}(L^{OH})](BF_4)_2x2H_2O$ ($C_{33}H_{34}B_2CuF_8N_6O_5$, MW: 831.82 g/mol): L^{OH} (0.05 g, 0.08 mmol, 1 eq) was dissolved in hot acetonitrile (4.0 ml), after addition anhydrous $Cu(BF)_4$ (0.02 g, 0.08 mmol, 1 eq) in acetonitrile (1.0 ml), the deep blue solution was heated to reflux once and stirring was continued at room temperature overnight. The blue solution was subjected to diethyl ether diffusion to obtain blue needles (39 mg, 54 % yield) suitable for x-ray diffraction. UV/Vvis λ = 630 nm (15873 cm^{-1}), ε = 112 M^{-1} cm^{-1}; CV:-671 mV (MeCN vs. Fc/Fc^{+}), -728 mV (H_2O vs. $K_3[Fe(CN)_6]$). Elemental analysis (report no. 32312) calc. (%): C(45.67), H(4.41), N(9.68); obs. (%) C(45.67), H(4.52), N(9.72).

*$[Cu^{II}(L)](ClO_4)_2xMeOH$***.** A suspension of L (0.15 g, 253.10 µmol, 1 eq) in MeOH (1.5 ml) was combined with a solution of $Cu(ClO_4)_2$ x 6 H_2O in MeOH/H_2O (1:1, 3.0 ml) and the resulting blue solution was refluxed for 60 minutes. After the solution was concentrated to one half of the initial volume and stored at +4 °C the product crystallized as blue plates (180 mg, 80 % yield). CV:-678 mV (MeCN vs. Fc/Fc^{+}). Elemental analysis (report no. 32341) calc. (%): C(46.03), H(4.09), N(9.47); obs. (%) C(45.85), H(4.26), N(9.63).

$[Fe(L^{OH})Cl](Cl)$. ($C_{33}H_{34}Cl_2F_eN_6O_5$, MW: 721.41 g/mol): L^{OH} (25mg, 0.04mmol, 1eq) was suspended in dry acetonitrile (2.0ml), anhydrous $FeCl_2$ was added under argon atmosphere, and the yellow solution was stirred at room temperature overnight. The yellow solution was subjected to diethyl ether diffusion to obtain yellow needles (15.9mg, 52%), suitable for x-ray diffraction. Elemental analysis ($C_{66}H_{74}Cl_4Fe_2N_{12}O_{13}$, report no. 32313) calc. C(52.96), H(4.98), N(11.23), obs. C(53.03), H(4.91), N(11.11), UV/vis (MeCN): λ = 412 nm (24271 cm^{-1}), ε = 1381 M^{-1} cm^{-1}, 341 nm (29326 cm^{-1}), ε = 1712 M^{-1} cm^{-1}, 259 nm (38610 cm^{-1}), ε = 10996 M^{-1} cm^{-1}; CV: 225 mV (MeCN vs. Fc/Fc^{+}), FAB-MS (NPOE-Matrix) m/z = 683.22 $[Fe(L^{OH})(Cl)]^{+}$, 701.24 $[Fe(L^{OH})(Cl)]^{+}$+H_2O, 715.28 $[Fe(L^{OH})(Cl)]^{+}$+MeOH.

$[Fe(L)(OMe)](ClO_4)_2$.:L (50.0mg, 0.08mmol, 1eq) was suspended in methanol (4.0ml), $Fe(ClO_4)_2$ (41mg, 0.17mmol, 2eq) was added and the yellow complex precipitated. The mixture was stirred at room temperature over-night, the solid was filtered of and dried under vacuum. The raw product was taken up in acetonitrile and subjected to diethylether diffusion to obtain yellow-brown needles (36mg, 49%), suitable for x-ray diffraction. Evans-NMR: μ_{eff}=5.1882 B.M., molar susceptibility 1.1415·10^{-2} cm^3/mol.

$[Fe(L)(HOMe)](BF_4)_2$: Under argon atmosphere L (100mg, 0.17mmol, 1eq) was stirred with $Fe(BF_4)_2 \cdot 6H_2O$ (57mg, 0.17mmol, 1eq) in methanol (3.0ml) at room temperature over-night. The yellow solution was subjected to diethylether diffusion to obtain yellow needles (78mg, 54%) suitable for x-ray diffraction. Elemental analysis calc. C(46.67), H(4.41), N(9.68), obs. C(45.76), H(4.52), N(9.72), UV/vis (MeCN): λ = 364 nm (27472 cm^{-1}), ε = 1245 M^{-1} cm^{-1}, CV: 474 mV (H_2O vs. $K_3[Fe(CN)_6]$), Evans-NMR: μ_{eff}=4.9613 B.M., molar susceptibility $1.0438 \cdot 10^{-2}$ cm^3/mol.

$[MnCl(L)]_2[MnCl_4]$. L (50.0mg, 0.08mmol, 1eq) was suspended in acetonitrile (2.0ml) and heated to 50°C until complete solution of the ligand. $MnCl_2 \cdot 4H_2O$ (17.0mg, 0.08mmol, 1eq) in acetonitrile/methanol 1:1 (2.0ml) was added, and the colorless solution was stirred at room temperature overnight. The solvent was evaporated the residue was redissolved in methanol. The supernatant was separated and subjected to diethyl ether diffusion, to obtain colorless needles (33mg, 56%), suitable for x-ray diffraction. Elemental analysis calc. C(48.18), H(4.97), N(9.63), obs. C(48.13), H(4.55), N(9.63), magnetic susceptibility: 4.168 $cm^3 K mol^{-1}$, CV: (MeCN) 791mV (vs. Fc/Fc^+).

Electronic Supporting Information.

CCDC 1030274-1030279 contains the supplementary crystallographic data for this paper. These data can be obtained free of charge from The Cambridge Crystallographic Data Centre via www.ccdc.cam.ac.uk/data_request/cif. The ESI also contains spectroscopic data of the compounds described.

Acknowledgements.

Financial support by the German Science Foundation (DFG), the University of Heidelberg and the Helmholtz Association (funding through the Helmholtz Virtual Institute NanoTracking, Agreement Number VH-VI-421 is gratefully acknowledged.

References.

1. C. Mannich and P. Mohs, *Chem. Ber.*, 1930, **B63**, 608-612.
2. P. Comba and M. Kerscher, *Coord. Chem. Rev.*, 2009, **253**, 564-574.
3. R. H. Blessing, *Acta Cryst.*, 1995, **A51**, 33-38.
4. P. Comba, M. Merz and H. Pritzkow, *Eur. J. Inorg. Chem.*, 2003, 1711-1718.

5. P. Comba, C. Lang, C. Lopez de Laorden, A. Muruganantham, G. Rajaraman, H. Wadepohl and M. Zajaczkowski, *Chem. Eur. J.*, 2008, **14**, 5313-5328.
6. P. Comba, C. Haaf, A. Lienke, A. Muruganantham and H. Wadepohl, *Chem. Eur. J.*, 2009, **15**, 10880-10887.
7. J. Benet-Buchholz, P. Comba, A. Llobet, S. Roeser, P. Vadivelu and S. Wiesner, *Dalton Trans.*, 2010, **39**, 3315.
8. J. Madhavan, P. Comba, M. Maurer, P. Vadivelu and V. Venuvanalingham, *Dalton Trans. (Special Issue Computational Chemistry of Inorganic Systems)*, 2011, **40**, 11276-11281.
9. F. Althoff, K. Benzing, P. Comba, C. McRoberts, D. R. Boyd, S. Greiner and F. Keppler, *Nature Comm., DOI:10.1038/ncomms5205*, 2014, **5**, 4205.
10. J. Bautz, P. Comba, C. Lopez de Laorden, M. Menzel and G. Rajaraman, *Angew. Chem. Int. Ed.*, 2007, **46**, 8067.
11. P. Comba, M. Maurer and P. Vadivelu, *Inorg. Chem.*, 2009, **48**, 10389-10396.
12. P. Comba and S. Wunderlich, *Chem. Eur. J.*, 2010, **16**, 7293-7299.
13. M. Atanasov, C. Busche, P. Comba, F. El Hallak, B. Martin, G. Rajaraman, J. van Slageren and H. Wadepohl, *Inorg. Chem.*, 2008, **47**, 8112.
14. M. Atanasov, P. Comba, G. R. Hanson, S. Hausberg, S. Helmle and H. Wadepohl, *Inorg. Chem.*, 2011, **50**, 6890-6901.
15. M. Atanasov, P. Comba and S. Helmle, *Inorg. Chem.*, 2012, **51**, 9357-9368.
16. M. Atanasov, P. Comba, S. Helmle, D. Müller and F. Neese, *Inorg. Chem.*, 2012, **51**, 12324-12335.
17. D. S. C. Black, M. A. Horsham and M. Rose, *Tetrahedron*, 1995, **51(16)**, 4819-4828.
18. P. Comba, S. Hunoldt, M. Morgen, J. Pietzsch, H. Stephan and H. Wadepohl, *Inorg. Chem.*, 2013, **52**, 8131-8143.
19. P. Comba, M. Kubeil, J. Pietzsch, H. Rudolf, H. Stephan and K. Zarschler, *Inorg. Chem.*, 2014, **53**, 6698-6707.
20. S. Juran, M. Walther, H. Stephan, R. Bergmann, J. Steinbach, W. Kraus, F. Emmerling and P. Comba, *Bioconjugate Chem.*, 2009, **20**, 347-359.
21. C. Busche, P. Comba, A. Mayboroda and H. Wadepohl, *Eur. J. Inorg. Chem.*, 2010, 1295-1302.
22. P. Comba, G. Haberhauer, D.-P. Herten, E. Kimmle, K. Kowski, M. Morgen, A. Rybina, G. Storch and H. Wadepohl, *Chem. Comm., in preparation*.
23. C. Nájera, J. Gil-Moltó and S. Karström, *Adv. Synth. Catal.*, 2000, **346**, 1798-1811.
24. G. Roelfes, V. Vrajmasu, K. Chen, R. Y. N. Ho, J. Rohde, C. Zondervan, R. M. la Crois, E. P. Schudde, M. Lutz, A. L. Spek, R. Hage, B. Feringa, E. Munck and L. Que Jr., *Inorg. Chem.*, 2003, **42**, 2639-2653.
25. P. Comba, H. Wadepohl and S. Wiesner, *Eur. J. Inorg. Chem.*, 2011, 2610-2615.
26. H. Börzel, P. Comba, K. S. Hagen, M. Kerscher, H. Pritzkow, M. Schatz, S. Schindler and O. Walter, *Inorg. Chem.*, 2002, **41**, 5440.
27. P. Comba, M. Kerscher, M. Merz, V. Müller, H. Pritzkow, R. Remenyi, W. Schiek and Y. Xiong, *Chem. Eur. J.*, 2002, **8**, 5750-5760.
28. C. Bleiholder, H. Börzel, P. Comba, R. Ferrari, A. Heydt, M. Kerscher, S. Kuwata, G. Laurenczy, G. A. Lawrance, A. Lienke, B. Martin, M. Merz, B. Nuber and H. Pritzkow, *Inorg. Chem.*, 2005, **44**, 8145-8155.
29. P. Comba, M. Kerscher and W. Schiek, *Prog. Inorg. Chem.*, 2007, **55**, 613-704.
30. K. Born, P. Comba, R. Ferrari, S. Kuwata, G. A. Lawrance and H. Wadepohl, *Inorg. Chem.*, 2007, **46**, 458-464.
31. E. A. Ambundo, M.-V. Deydier, A. J. Grall, N. Agnera-Vega, L. T. Dressel, T. H. Cooper, N. J. Heeg, L. A. Ochrymowycz and D. B. Rorabacher *Inorg. Chem.*, 1999, **38**, 4233-4242.
32. P. Comba, M. Morgen and H. Wadepohl, *Inorg. Chem.*, 2013, **52**, 6481-6501.
33. H. Börzel, P. Comba, K. S. Hagen, M. Merz, Y. D. Lampeka, A. Lienke, G. Linti, H. Pritzkow and L. V. Tsymbal, *Inorg. Chim. Acta*, 2002, **337**, 407-419.

34. J. L. Kolanowski, E. Jeanneau, R. Steinhoff and J. Hasserodt, *Chem. Eur. J.*, 2013, **19**, 8839-8884?
35. S. Wiesner, Thesis, Heidelberg, 2009.
36. P. Comba, H. Wadepohl and A. Waleska, *Aust. J. Chem. (Heron 6 Special Issue)*, 2014, **67**, 398-404.
37. The oxidation of the FeII complex by dioxygen itself is an interesting process and, according to recent studies on "oxygen activation" by FeII bispidine complexes (e.g., with L1) this probably is a reaction initiated by carbon-based radical impurities.[38]
38. P. Comba, Y.-M. Lee, W. Nam and A. Waleska, *Chem. Commun. (Special Web Themed Issue 'Biological Oxidation Reactions)*, 2014, **50**, 412-414.
39. G. Roelfes, M. Lubben, K. Chen, R. Y. N. Ho, A. Meetsma, S. Genseberger, R. M. Hermant, R. Hage, S. K. Mandal, V. G. Young Jr., Y. Zang, H. Kooijman, A. L. Spek, L. Que Jr. and B. L. Feringa, *Inorg. Chem.*, 1999, **38**, 1929-1936.
40. N. A. Ortega-Villar, M. C. Munoz and J. A. Real, *Eur. J. Inorg. Chem.*, 2010, 5563.
41. S. Helmle, Thesis, Heidelberg, 2010.
42. S. Richards, B. Pedersen, J. V. Silverton and J. L. Hoard, *Inorg. Chem.*, 1964, **3**, 27-33.
43. S. Zetter, M. W. Grant, E. J. Wood, H. W. Dodgen and J. P. Hunt, *Inorg. Chem.*, 1972, **11**, 2701-2706.
44. A. Dees, A. Zahl, R. Puchta, N. J. R. van Eikema Hommes, F. W. Heinemann and I. Ivanovic-Burmazovic, *Inorg. Chem.*, 2007, **46**, 2459-2470.
45. D. V. R. Rao and S. K. Naik, *Curr. Science* 1964, **33**, 109.
46. P. Comba, C. Lopez de Laorden and H. Pritzkow, *Helv. Chim. Acta*, 2005, **88**, 647-664.
47. P. Comba, M. Kerscher, G. A. Lawrance, B. Martin, H. Wadepohl and S. Wunderlich, *Angew. Chem. Int. Ed.*, 2008, **47**, 4743.
48. D. Wang and G. R. Hanson, *J. Magn. Reson. A*, 1995, **117**, 1-8.
49. D. Wang and G. R. Hanson, *Appl. Magn. Reson.*, 1996, **11**, 401-415.
50. *SAINT*, Bruker AXS, Karlsruhe, 1997-2013.
51. CrysAlisPro, Agilent Technologies, UK Ltd., Oxford, 2011-2013.
52. G. M. Sheldrick, Bruker AXS, Karlsruhe, 2004-2014.
53. CrysAlisPro, Agilent Technologies UK Ltd., Oxford, SCALE3 ABSPACK CrysAlisPro, 2011-2014.
54. G. M. Sheldrick, University Göttingen, Göttingen, 1997, p. Program for structure solution.
55. G. M. Sheldrick, *Acta Cryst.*, 2008, **A64**, 112-122.
56. L. Palatinus and G. Chapuis, *J. Appl. Cryst.*, 2007, **40**, 786-790.
57. L. Palatinus, *SUPERFLIP*, EPF Lausanne, Switzerland, 2007.
58. G. M. Sheldrick, University of Göttingen, 2012-2014.
59. M. Nardelli, *J. Appl. Cryst.*, 1982, **6**, 139.
60. M. Nardelli, *J. Appl. Cryst.*, 1999, **32**, 563.
61. C. J. Cramer, *Essentials of Computational Chemistry, 2nd Ed.*, Wiley-VCH, New York, 2004.
62. P. v. d. Sluis and A. L. Spek, *Acta Cryst.*, 1990, **A46**, 194-201.
63. R. W. Grosse-Kunstleve, N. K. Sauter, N. W. Moriarty and P. D. Adams, *J. Appl. Crystallography* 2002, **35**, 126-136.
64. A. L. Spek, Utrecht University, The Netherlands, 2003.
65. A. L. Spek, *J. Appl. Cryst.*, 2003, **36**, 7-13.
66. J. Jochims, *Monatshefte fuer Chemie*, 1963, **4**, 677.
67. E. Niemers and R. Hiltman, *Synthesis*, 1976, 593.
68. S. Groni, C. Hureau, R. Guillot, G. BLondin, G. Blain and E. Anxolabéhère-Mallart, *Inorg. Chem.*, 2008, **47**, 11783.
69. P. Comba, B. Kanellakopulos, C. Katsichtis, A. Lienke, H. Pritzkow and F. Rominger, *J. Chem. Soc., Dalton Trans.*, 1998, 3997-4002.
70. V. V. Pavlishchuk and A. W. Addison, *Inorg. Chim. Acta*, 2000, **298**, 97-102.
71. B. Drahos, I. Lukes and E. Toth, *Eur. J. Inorg. Chem.*, 2012, **12**, 1975.

Table 1. Selected distances and angles of the Cu^{II} complexes of L and L^{OH} in comparison with those of L^1 and L^2.[4, 28]

distances [Å]	$[Cu^{II}(L)]^{2+}$	$[Cu^{II}(L^{OH})]^{2+}$	$[Cu^{II}(L^1)Cl]^{+}$	$[Cu(L^2)]^{2+}$
Cu–N3	2.003(3)	1.993(2)	2.036(2)	2.087(3)
Cu–N7	2.237(3)	2.233(2)	2.368(2)	2.045(3)
Cu–py1	2.047(3)	2.052(2)	2.028(2)	2.573(3)
Cu–py2	2.040(3)	2.039(2)	2.029(2)	2.208(3)
Cu–py3	1.984(3)	1.976(2)	2.029(2)	2.028(3)
Cu–py4	3.893(3)	3.854(2)	—	[2.009(3)]
Cu-F11	2.637(3)	2.653(2)	—	—
N3···N7	2.934(5)	2.930(3)	2.915	2.83
py1···py2	3.986(5)	3.994(3)	3.995	4.67
angles [°]				
N3–Cu–N7	87.41(13)	87.57(8)	82.53(6)	86.43(12)
N3–Cu–py1	80.89(14)	80.84(9)	81.39(7)	—
N3–Cu–py2	80.73(14)	80.79(9)	80.94(7)	—
N3–Cu–py3	168.79(14)	169.18(9)	160.82(7)	154.39(13)
N7–Cu–py1	104.53(14)	103.72(8)	88.32(6)	—
N7–Cu–py2	91.97(12)	92.52(8)	98.43(6)	—
py1–Cu–py2	154.62(13)	154.84(9)	160.07(7)	148.53
N7–Cu–py3	82.81(12)	83.11(8)	79.27(7)	—
py1–Cu–py3	96.2(1)	96.02(9)	110.00(6)	
py2–Cu–py3	105.0(1)	105.02(9)	97.02(6)	

Table 2. Redox potentials (MeCN vs. Fc/Fc+, vs. $Ag/AgNO_3$; H_2O vs. $K_3[Fe(CN)_6]$ [a] or vs. $Ag/AgCl$[b]) and spectroscopic data of the Cu^{II} complexes of L and L^{OH}, in comparison with other Cu^{II} bispidine complexes.[2, 28, 30, 44]

	Cu^{I}/Cu^{II} [mV]		*dd Cu^{II} [nm]*	*EPR ($g_{x,y}$, g_z; $A_{x,y}$, A_z)*
	MeCN	H_2O	MeOH (ε [M^{-1} cm^{-1}])	MeOH/EtOH, 5K A in $10^{-4}cm^{-1}$, SOPHE simulation[45, 46]
$[Cu(L)](BF_4)_2$	-651 (-602)	-786[a]; -515[b]	626 (119)	2.061, 2.237; 8.5, 172.9
$[Cu(L^{OH})](BF_4)_2$	-671 (-538)	-730[a]; -459[b]	630 (112)	—
$[Cu(L)](ClO_4)_2$	-678 (-594)	—	—	—
$[Cu(L^1)]^{2+}$	-776 (-603)	-523[b]	617 (108)	2.060, 2.217; -,178
$[Cu(L^2)]^{2+}$	-745 (-573)	-502[b]	620 (125)	2.069, 2.208; - ,169
$[Cu(L^3)]^{2+}$	—	-433[b]	573	—

Table 3. Selected bond distances and angles of the Fe^{II} and Fe^{III} complexes of L, L^{OH} and other bispidine complexes.

distances [Å]	$[Fe^{II}(L)OHMe]^{2+}$	$[Fe^{II}(L^{OH})Cl]^{+}$	$[Fe^{II}(L^{1})OHMe]^{2+}$ [41]	$[Fe^{II}(L^{1})Cl]^{+}$ [33]	$[Fe^{II}(L^{2})SO_4]$ [33]	$[Fe^{II}(L^{3})Cl]^{+}$ [25]	$[Fe^{III}(L)OMe]^{2+}$	$[Fe^{III}(L^{1'})OCH_2CF_3]^{2+}$ [a] [36]
Fe–N3	2.289(2)	2.235(2)	2.177(3)	2.194(2)	2.215(9)	2.213(2)	2.1916(15)	2.202(2)
Fe–N7	2.2482(18)	2.309(2)	2.293(3)	2.362(2)	2.274(10)	2.342(2)	2.2951(15)	2.193(2)
Fe–py1	2.265(2)	2.294(2)	2.163(3)	2.182(2)	2.206(10)	2.232(2)	2.2281(17)	2.106(2)
Fe–py2	2.184(2)	2.189(2)	2.231(3)	2.142(2)	2.172(10)	2.173(2)	2.1425(16)	2.095(2)
Fe–py3	2.209(2)	2.174(2)	2.110(3)	2.134(2)	2.195(10)	2.143(2)	2.1099(16)	2.093(2)
Fe–py4	3.025(1)	3.352(3)	—	—	1.957(8)	4.058(3) [d]	3.240(2)	—
Fe–X_A	2.0939(19) [b]	2.3954(7) [b]	2.120(3) [b]	2.416(1) [b]	1.957(8) [c]	2.3616(7) [b]	1.7923(14) [b]	1.791(2) [c]
N3 ··· N7	2.897(6)	2.908(6)	2.923	2.879(2)	2.883(9	2.938(3)	2.861(2)	2.893(3)
py1 ··· py2	4.150(6)	4.260(6)		4.195(2)	4.245(10)	4.265(3)	4.177(2)	4.090(3)
angles [°]								
N3–Fe–N7	79.50(7)	79.44(7)	81.6(1)	78.27(5)	79.94(3)	80.29(7)	79.19(6)	82.33(7)
N3–Fe–py1	70.92(7)	72.56(8)	77.0(1)	76.00(5)	76.32(3)	76.07(8)	73.59(6)	
N3–Fe–py2	72.05(7)	73.59(8)	76.5(1)	76.48(6)	76.01(3)	75.35(8)	74.18(6)	
N7–Fe–py1	99.06(7)	97.21(8)		94.12(5)	89.18(3)	87.21(7)	95.66(6)	
N7–Fe–py2	93.61(7)	89.51(8)		86.15(5)	91.75(3)	92.41(7)	89.48(6)	
py1–Fe–py2	137.70(7)	143.54(8)		151.82(6)	151.70(4)	151.05(8)	145.73(5)	153.64(8)
py1–Fe–py3	84.87(8)	86.56(8)		93.68(6)	92.1(4)	92.18(8)	86.85(6)	
py2–Fe–py3	137.41(8)	129.70(9)		113.73(6)	77.1(4)	115.83(8)	127.20(6)	
Fe–O–CH_3	130.97(18)	—	—	—	—	—	149.12(12)	

[a] $L^{1'}$ is an isomer to L^1 with the pyridine group attached to N3 instead of N7
[b] *trans* zu N7
[c]) *trans* zu N3
[d] C-atom of the phenylring pointing in direction of the metal center

Table 4. Redox potentials (MeCN vs. Fc/Fc+ [a]; vs. $Ag/AgNO_3$ [b]; H_2O vs. $K_3[Fe(CN)_6]$ [c]; vs. Ag/AgCl [b]) and spectroscopic data of the Fe^{II} complexes of L and L^{OH}, in comparison with other Fe^{II} bispidine complexes. [33, 35, 36]

	Fe^{III}/Fe^{II} [mV]			dd Fe^{II} [nm]
	H_2O[a]	MeOH[b]	MeCN	MeCN
$[Fe(L)OHMe]^{2+}$	474		—	364
$[Fe(L^{OH})Cl]^{+}$	225		222[c]	341, 412
$[Fe(L^{1})Cl]^{2+}$	—	156	—	309; 402
$[Fe(L^{2})]^{2+}$	—	—	661[b]	376; 402; 457; 564
$[Fe(L^{3})OTf]^{+}$	—		773[c]	—

[a] vs. Fc/Fc^{+}; [b] vs. $Ag/AgNO_3$; [c] vs. $K_3[Fe(CN)_6]$

Table 5. Selected structural parameters of $[Mn^{II}(L)Cl]^+$ and relevant data for comparison.

distance [Å]	$[Mn^{II}(L)Cl]^{+}$ a)		$[Mn^{II}(L^1)Cl]^{+}$ 41	$[Mn^{II}(tpen)Cl]^{+}$ b)
Mn–N3	2.435(2)	2.485(2)	2.2829(1)	2.485(2)
Mn–N7	2.326(2)	2.344(2)	2.4151(1)	2.444(2)
Mn–py1	2.307(2)	2.362(2)	2.2714(1)	2.262(2)
Mn–py2	2.389(2)	2.342(2)	2.2622(1)	2.490(2)
Mn–py3	2.346(2)	2.415(2)	2.1910	2.297(2)
Mn–py4	2.647(2)	2.529(2)	—	2.498(2)
Mn–Cl	2.3933(8)	2.4064(8)	2.3914(1)(2)	2.4544(7)
N3···N7	2.926(3)	2.926(3)	2.943	—
py1···py2	4.273(3)	4.246(3)	—	—
angle [°]				
N3–Mn–N7	75.80(7)	74.51(6)	77.507(2)	—
N3–Mn–py1	68.29(7)	66.82(7)	73.599(2)	—
N3–Mn–py2	67.51(7)	66.81(7)	74.010(2)	—
N3–Mn–py3	133.62(7)	132.42(7)	149.085(2)	—
N3–Mn–py4	127.55(7)	127.15(7)	—	—
N7–Mn–py1	93.98(7)	92.24(7)	—	—
N7–Mn–py2	94.85(7)	94.95(7)	85.5(1)	—
N7–Mn–py4	69.62(7)	70.63(7)	—	—
N7–Mn–py3	73.15(7)	73.16(7)	—	—
py1–Mn–py2	131.00(8)	129.00(7)	144.4(1)	—
N7–Mn–Cl	164.62(6)	166.62(7)	112.147(1)	139.44(6)
py1–Mn–py4	75.98(8)	80.55(8)		
py3–Mn–py4	70.56(7)	71.45(8)		
py2–Mn–py3	81.76(8)	77.93(8)		

a) two independent molecules

b) tpen = N,N,N',N'-tetrakis(2-pyridylmethyl)ethylene-1,2-diamine[68]

Table 6. Redox potentials of $[Mn(L)Cl]^+$ relevant data for comparison in MeCN, vs. SCE.

	$Mn^{II/III}$ [mV]
$[Mn(L)Cl]^+$	1171[d]
$Mn(L'')Cl_2$ [a]	911[a]
$[Mn(tpen)Cl]^+$ [b]	1050
$[Mn(NOTA)]^-$ [c]	496 [e]
$[Mn(EDTA)]^{2-}$ [c]	566 [e]

[a] L'' is a tetradentate bispidine derivative;[69] $E(Ag/AgNO_3)$ = 343mV vs. SCE [70]

[b] tpen = N,N,N',N'-tetrakis(2-pyridylmethyl)ethylene-1,2-diamine [68]

[c] NOTA = 1,4,7-triacetato-1,4,7-triazanonane; EDTA = N,N,N',N'-tetraacetatoethylene-1,2-diamine[71]

[d] $E(Fc/Fc^+)$ = 380mV vs. SCE[70]

[e] E(SHE) = -244 vs. SCE [70]

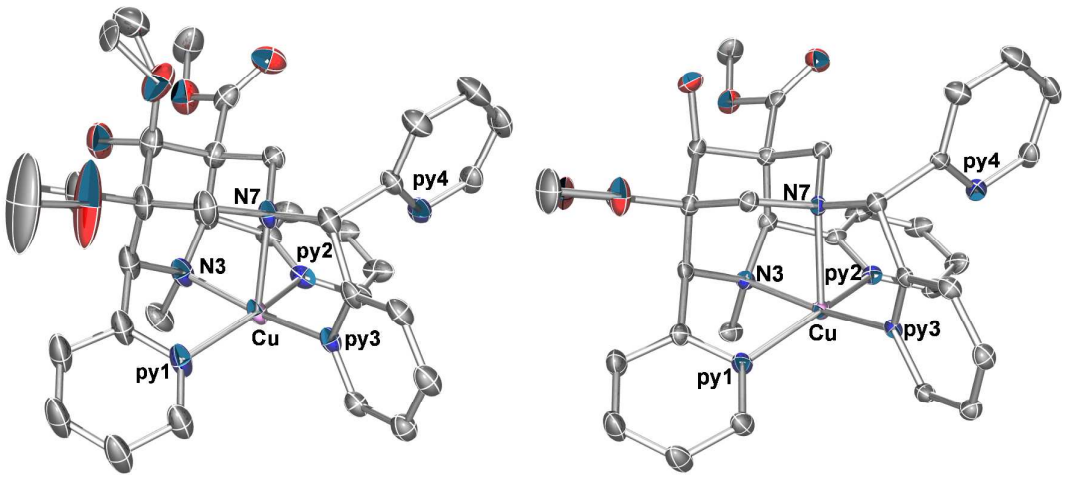

Figure 1. ORTEP plots of $[Cu^{II}(L)]^{2+}$ (left) and $[Cu^{II}(L^{OH})]^{2+}$ (right), hydrogen atoms are omitted for clarity, ellipsoids are shown with 50% probability.

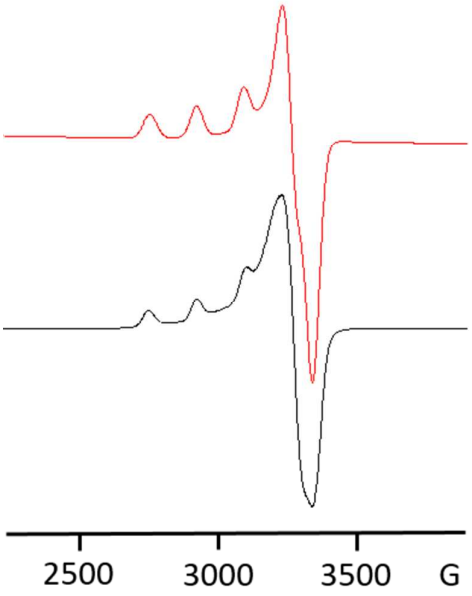

Figure 2. X-band EPR spectrum of $[Cu^{II}(L)]^{2+}$ in MeOH/EtOH (9:1) at 5 K and 9.423336 GHz, black line (bottom): experimental spectrum, red line (top) simulated spectrum.

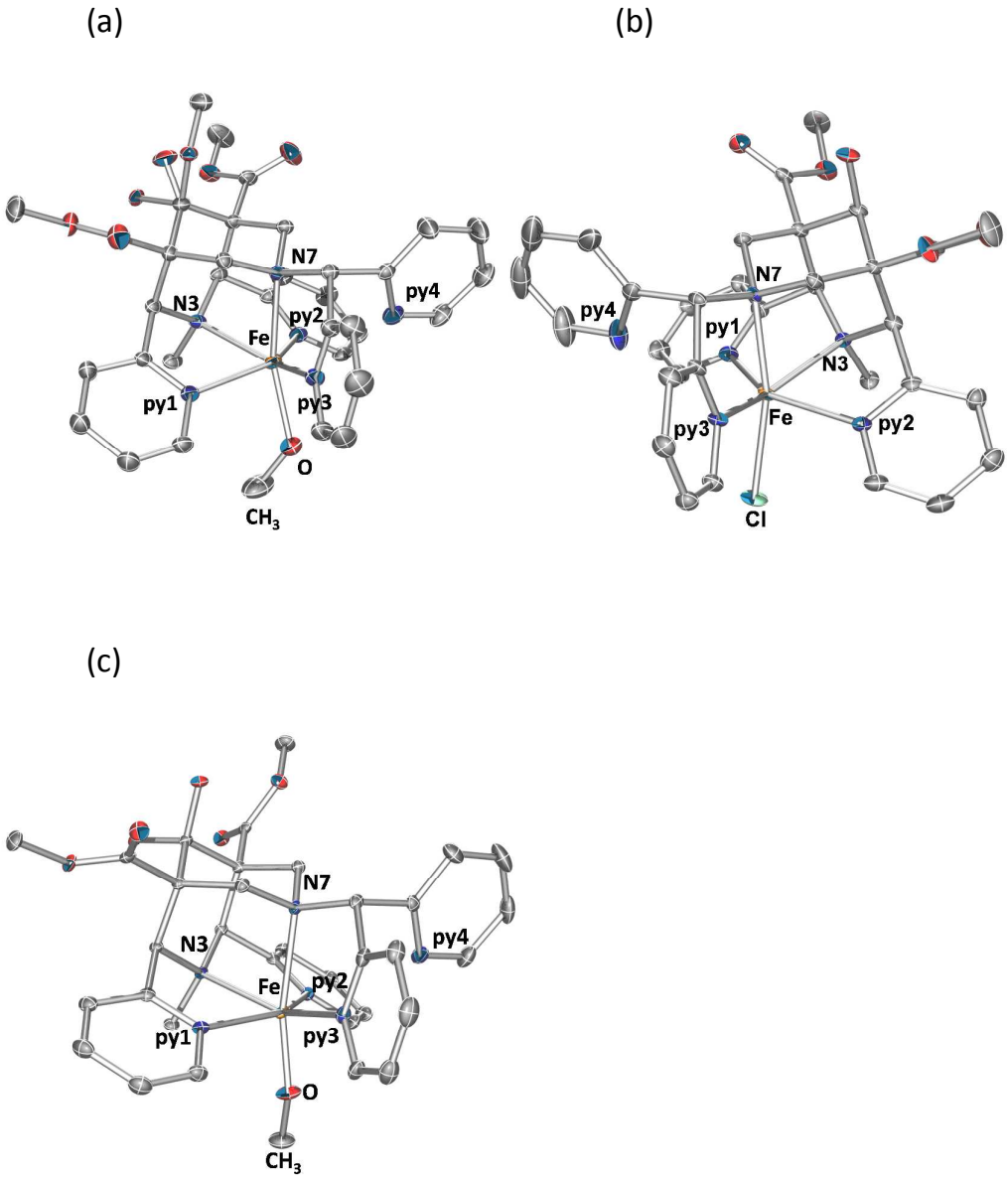

Figure 3. ORTEP plots of the complex cations (a) $[Fe^{II}(L)OHMe]^{2+}$, (b) $[Fe^{II}(L^{OH})Cl]^{+}$, and (c) $[Fe^{III}(L)OMe]^{2+}$; hydrogen atoms are omitted for clarity, ellipsoids are shown with 50% probability level.

(a)

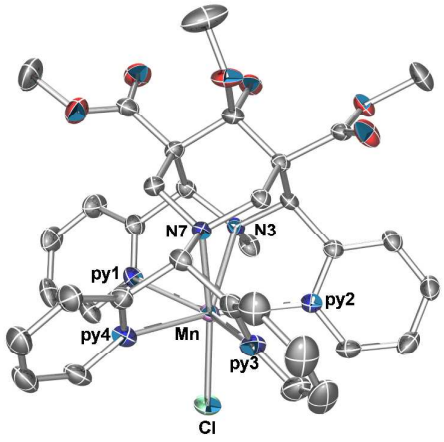

(b)

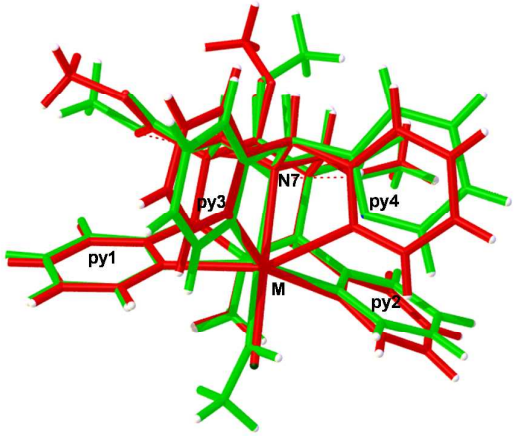

Figure 4. (a) ORTEP plot of the complex cation $[Mn^{II}(L)(Cl)]^{+}$ (only one of the two independent molecules is shown, hydrogen atoms are omitted for clarity, ellipsoids are shown with 50% probability level); (b) overlay plot of $[Mn^{II}(L)(Cl)]^{+}$ (red, M=Mn^{II}) and $[Fe^{II}(L)(HOMe)]^{2+}$ (green, M=Fe^{II}).

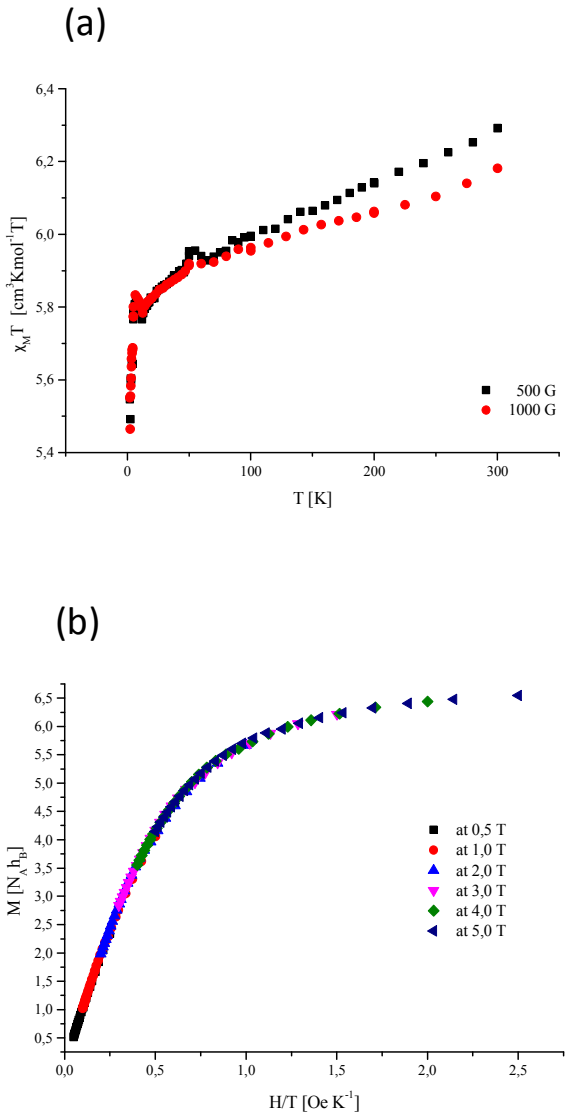

Figure 5. (a) Temperature depencent suszeptibility and (b) reduced magnetization of $[Mn^{II}(L)(Cl)]_2[MnCl_4]$.

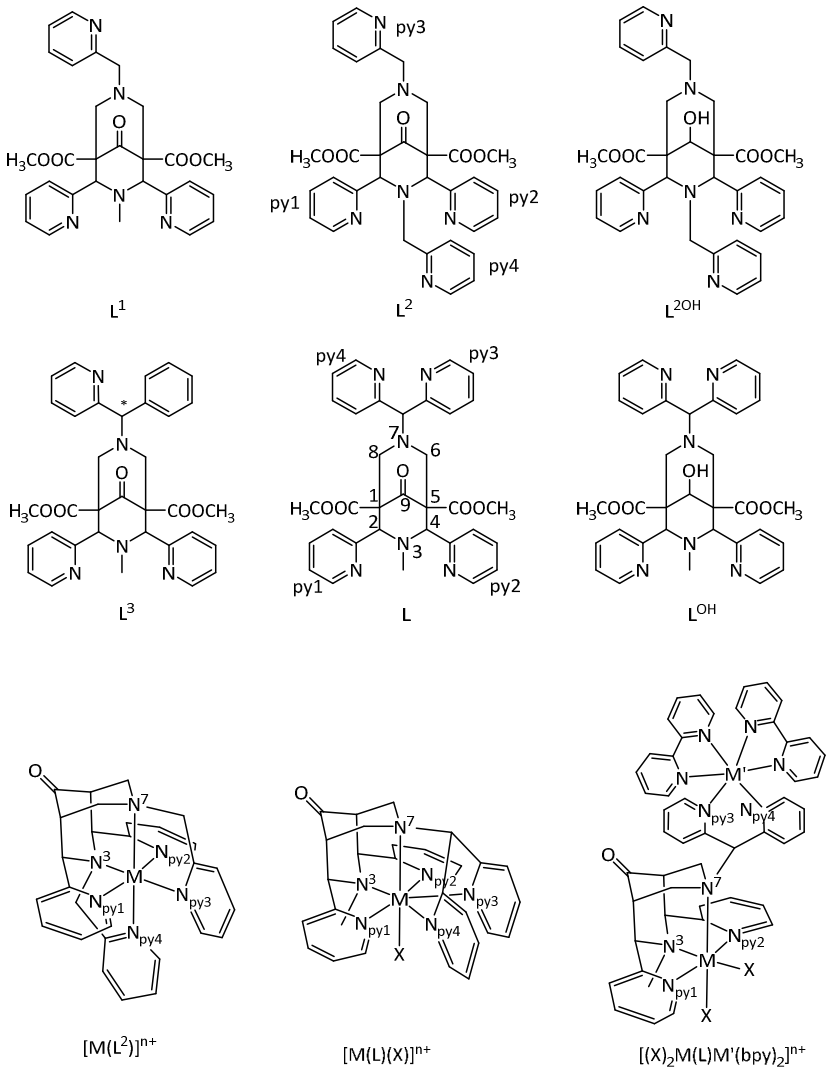

Chart 1. Ligands discussed in this publication, and the two isomeric hexacoordinate structures with L^2 and L (if X = void), as well as the two coordination modes (mono- and dinucleating) of the hexadentate bispidine L.

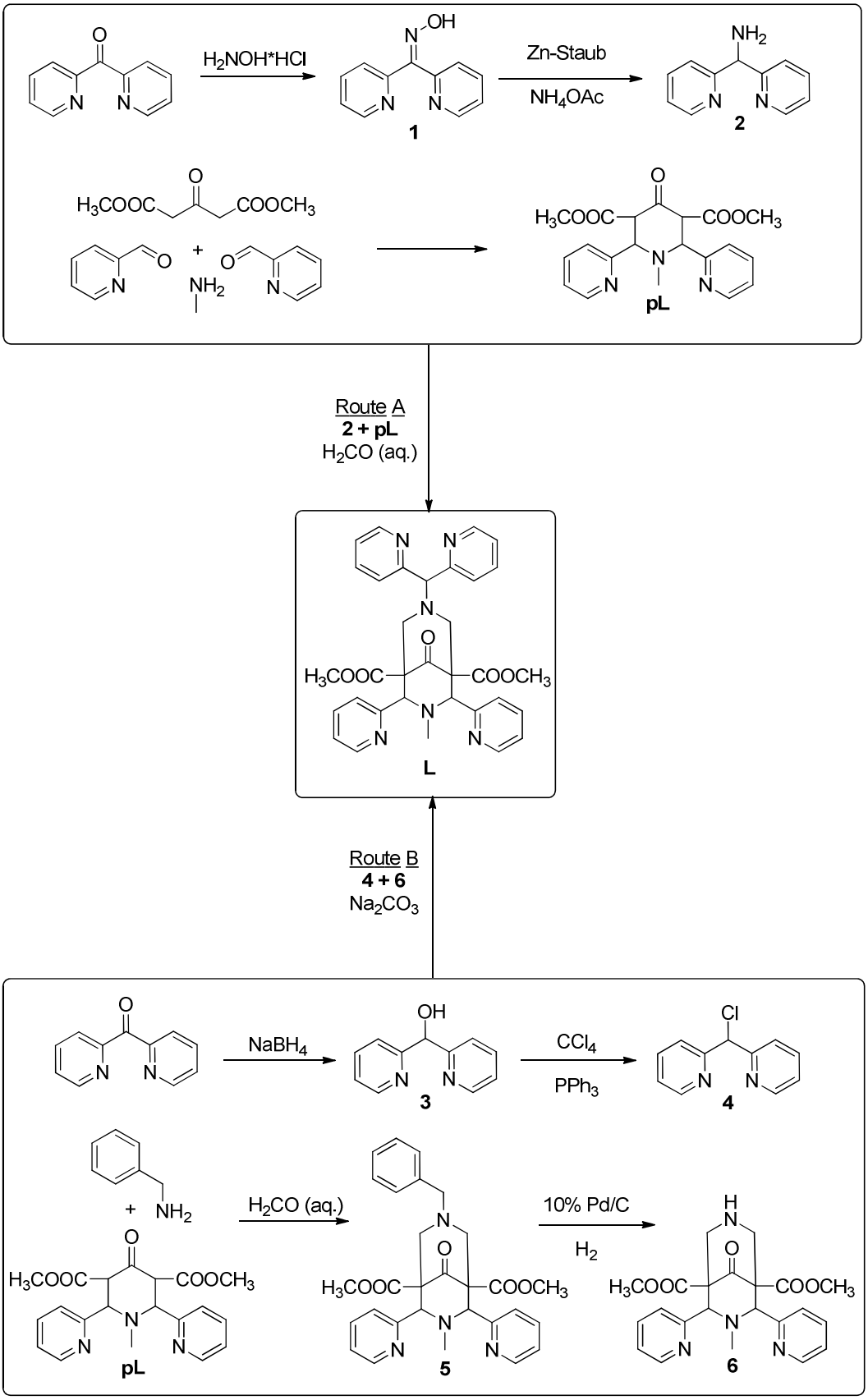

Scheme 1. Two different synthetic routes to Ligand L.

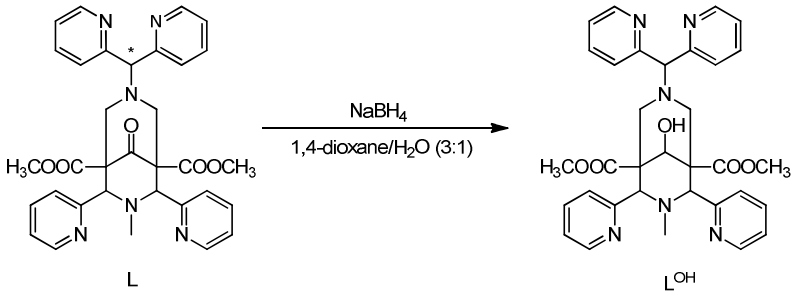

Scheme 2. Reduction of L to L^{OH}

Graphical Abstract.

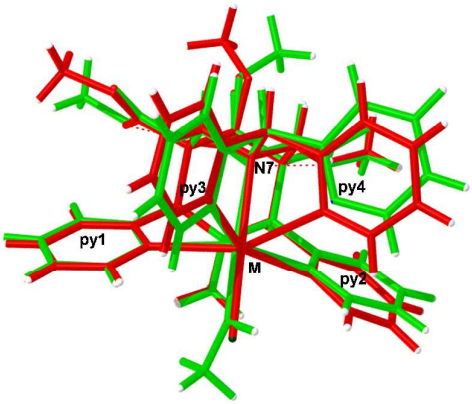

Table of contents entry.

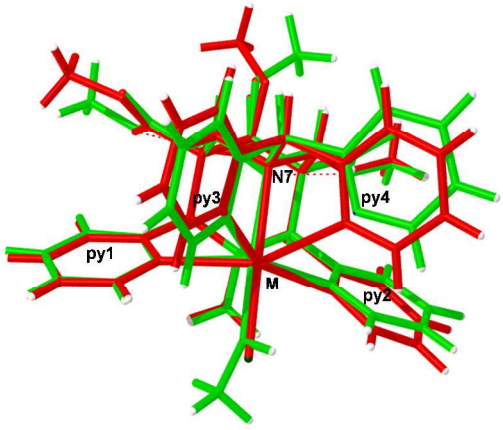

With the hexadentate bispidine ligand, the Cu^{II} and Fe^{II} (red) complexes are hexacoordinated with a semi-coordinated py4, the Mn^{II} complex (green) is heptacoordinated.